Proceedings of ASME Turbo Expo 2016: Turbomachinery Technical Conference and Exposition
GT2016
June 13 – 17, 2016, Seoul, South Korea

GT2016-56307

ROTATING HEAT TRANSFER MEASUREMENTS ON A MULTI-PASS INTERNAL COOLING CHANNEL - II EXPERIMENTAL TESTS

Fabio Pagnacco, Luca Furlani, Alessandro Armellini, Luca Casarsa
Università degli Studi di Udine
Dipartimento di Ingegneria Elettrica Gestionale e Meccanica
33100 Udine, Italy
Email: luca.casarsa@uniud.it

Anthony Davis
Siemens Industrial Turbomachinery Ltd
Ruston House, Waterside South, LN5 7FD
Lincoln, England

ABSTRACT

The present contribution is focused on heat transfer measurements on internal cooling channels of a high pressure gas turbine blade in static and rotating conditions.

A novel rig designed for the specific purpose was used to assess the heat transfer coefficients on a full internal cooling scheme of an idealized blade. The channel has a multi-pass design. Coolant enters at the blade hub in the leading edge region and move radially outwards inside a two-sided ribbed channel. The second passage is again a two-sided ribbed channel with a trapezoidal cross section of high aspect ratio, while inside the third leg low aspect-ratio cylindrical pin fins are arranged in a staggered configuration to promote flow turbulence. Inside the third passage, the coolant is progressively discharged at the blade trailing edge and finally at the blade tip. The test model differs with respect to the real design only because there is no curvature due to the blade camber. Conversely, the correct stagger angle of the real blade with respect to the rotation axis is preserved.

Experiments were performed for static and rotating conditions with engine similar conditions of Re=21000 and Ro=0.074, both defined at the channel inlet. Transient liquid crystal technique was used for the measurement of the heat transfer coefficient (HTC) on both pressure and suction sides internal surfaces of the channel. From the spatially resolved HTC maps available, it is possible to characterize the thermal performances of the whole passage and to highlight the effect of rotation.

INTRODUCTION

Many different cooling methods have been developed to ensure that the turbine blade metal temperatures are maintained at a level consistent with safe and economic airfoil service life. Adoption of internal cooling is the starting point to achieve this task. Coolant air is routed to serpentine passages within the airfoil and convectively removes heat from the blade. The spent coolant can be then exhausted in multiple ways: at the blade tip, through cooling holes or slots at the trailing edge or by film cooling holes in multiple locations on the airfoil surface. This necessary cooling flow has a strong impact on the turbine efficiency, therefore improving cooling technology is always a focus point of gas turbine industry research activity, as demonstrated by the large literature available.

Inside multi-pass channels different types of turbulent promoters are used to enhance heat transfer. The choice of which kind of turbulator to install is constrained by the channel cross section dimensions and aspect ratio, which in turns depends upon the blade region where the passage is located. Inclined ribs are usually found in the first legs, which have the task to cool leading edge and main body regions. Conversely, inside the thin trailing edge of the airfoil, pin-fin channels are prevalently adopted with combined benefits of structural integrity and heat transfer enhancements.

ROTATING HEAT TRANSFER, CURRENT STATE-OF-ART

Another important aspect that has to be taken into account in the design process of a cooling passage is the combined effect of turbulators, rotation, and channel orientation. The experimental and numerical results obtained by Hart [1], Lezius and Johnston [2], Speziale [3], and Speziale and Thangam [4] can be considered as the fundamental contributions describing the Coriolis effects on the flow field inside basic channel geometries

(square or rectangular channels with outward flow in orthogonal rotation, i.e. the rotation axis is parallel to the channel height). In these channel configurations, the effect of rotation consists in the development of secondary flow structures made of two symmetrical vortex cells. The number of vortex cells can increase depending on the channel aspect ratio. However, separation and reattachment of the recirculating structures occurs on the leading and trailing walls of the channel, respectively. This leads to a flow unbalance towards the trailing side and a consequent enhancement of heat transfer. On the opposite, thermal performance will reduce on the leading side. The reverse trend is true in radial inward flow passages. Wagner et al. [5] extended the work about rotational effects to rib-roughed channels with ribs installed on both leading and trailing walls. The results show how the local heat transfer coefficients can vary from 0.65 to 4.5 times the values for the fully-developed flow in the smooth passage, with the positive effect measured on the trailing side. The same general behavior is confirmed by [6], who considered a high aspect ratio (4:1) two pass channel with ribs skewed 45° to the flow and reported heat transfer data on a wide range of working conditions (Re=10.000-70.000, Ro=0-0.7).

As said, the above works refer to simplified geometries while more recent contributions clearly show how the flow structure can change significantly if the channel section is no longer rectangular. In [7] a triangular shaped smooth channel for leading edge cooling is investigated. By performing detailed PIV measurements and CFD simulations it is demonstrated that the secondary structures differ significantly to the ones found in rectangular channel. Separation and reattachment points do not occur anymore on the channel lateral walls, multiple vortex cells develop streamwise, with a significant impact on the heat transfer performance. Combined effect of ribs, rotation, and buoyancy are studied in [8] again inside a triangular channel. The results show a different behavior from the rectangular channel case [9].

In real turbines blades, channels are not always in orthogonal rotation, i.e. the leading and trailing surfaces are not parallel to the rotation axis, because of the blade shape and the channel location. In the experiments of [10] it is shown how the heat transfer inside a two-pass smooth square channel can vary with the channel orientation angle, the latter being defined as the angle between the channel outer wall in chord-wise direction and the channel rotation direction. The heat transfer inside a rectangular two-pass channel with 2:1 aspect ratio was studied by [11] for two channel orientations (90° and 45°) and smooth or ribbed walls. Again, it was reported how the channel orientation is important to heat transfer development and, in their particular case, it is beneficial to heat transfer augmentation on the leading surface of the first passage.

As already reported, pin-fins are normally used in blade cooling inside narrow channels at the trailing edge. The flow physics in a pin-fin channel is very complicated and three-dimensional in view of the complex and unsteady separation that takes place around the obstacles, and of the possible mutual interaction phenomena of wakes in staggered arrays of pins. This results in high sensitivity of heat transfer coefficients to pin-fin arrangement ([12] and [13], to cite few examples).

The scenario is further complicated by the progressive discharge of spent coolant through the trailing edge. The progressive flow rate reduction causes a reduction of the local Reynolds number with a detrimental effect on the heat transfer process [14]. Also, the reduction of bulk flow velocity determines the local increase of the rotation number, and rotational effects should therefore change in intensity while moving from hub to tip. However, studies about the effect of rotation in pin fins roughened channels ([14-16]) concluded that it is not significant. A justification is based on the large blockage effect pins-fins have on Coriolis induced secondary flows. On the other hand, the recent work [17] investigated the effect of the channel orientation with the use of pin fins. For two extreme values of channel orientation (namely 90° and 180°), a strong variation of heat transfer is reported. A critical value of Ro, which sets an abrupt change in Nu, is also identified. It is therefore evident the need for more detailed investigations about the thermal behavior of pin fin roughened channels under rotation.

The heat transfer performance inside the second and third legs can be significantly modified by the presence of the upstream turn. Indeed, inside the bend region complicated flow structures such as separation, recirculation, and secondary vortices arise, [18]. Adding rotation and channel orientation increase the complexity of the flow, resulting in different behavior if a tip or hub turn is considered [18, 19]. The extended literature available on bend regions flow & losses is still not sufficient to draw conclusion of general validity to be applied for design purposes.

Finally, the effects associated to the blade manufacturing process has to be considered. Gas turbine blades are manufactured by casting, and therefore it is difficult to ensure that the internal passages have sharp edges or perfectly squared ribs. Also, wearing out of the casting die due to ageing is an issue which results in rib rounding and filleting even in larger land-based gas turbine engines. Conversely, researchers have focused extensively on channels with sharp edged ribs, documenting heat transfer and friction loss characteristics for a variety of parameters. Only few studies are available on more realistic turbulators geometries and all demonstrated a deterioration in heat transfer due fillets at the base of the rib [20-22] or pin-fin [14]. However, in all cases, the effect is a reduction of the pressure losses.

From the literature review of above, it should be clear that the complexity of the modern internal cooling designs makes difficult to predict the expected thermal performances starting from the available knowledge. Indeed, the majority of the data refers to stereotyped geometrical configurations or the results cannot be projected straightforward to the engine because of lack of full similarity between experiments (real or virtual) and real engine conditions.

The present work investigates the rotational effects inside a three-pass channel for cooling of land based gas turbine engine. The geometry still brings some simplifications with respect to the real application, but the main features are considered, such as realistic cross section with rounded walls, angled ribs and

filleted pin fins. Channel orientation is consistent with the real application as well as the imposed flow split among the different coolant discharges.

NOMENCLATURE

Bo	buoyancy parameter
d	pin fin diameter
d_h	hydraulic diameter
HTC	heat transfer coefficient
k	air thermal conductivity
Nu	Nusselt number
Nu_0	reference Nusselt number
Pr	Prandtl number
R	rotation radius
Re	Reynolds number
Ro	rotation parameter
T_b	bulk flow temperature
T_{he}	temperature at the outlet of heat exchangers
T_i	initial flow temperature
T_w	wall temperature
U_b	bulk velocity
μ	air dynamic viscosity
ρ	air density
Θ	non dimensional temperature
Ω	rotational speed

EXPERIMENTAL SETUP

CHANNEL GEOMETRY

The test section is a model of a full internal cooling scheme of an idealized blade. Figure 1 reports a drawing of the test section and a view of its installation on the rig, the details of which are given in the next section. The cooling scheme has a multi-pass design where coolant enters at the blade hub in the leading edge region and moves radially outwards inside a two-sided ribbed channel (the ribs on the two sides are arranged in a line-on-line configuration). At the blade tip, part of the coolant is discharged through a dust hole (10% of inlet mass flow rate), while the greater part of it goes through a 180° bend and flows radially inwards inside the 2nd passage. This latter, is again a two-sided ribbed channel with a trapezoidal cross section of high aspect ratio. At the end of the second passage, another 180° bend diverts the flow inside the 3rd leg, where low aspect-ratio cylindrical pin fins (d/d_h = 0.34) are arranged in a staggered configuration to promote flow turbulence. Inside the 3rd passage, the coolant is progressively discharged through holes at the blade trailing edge (55% of inlet mass flow rate) and finally at the blade tip (35% of inlet mass flow rate). The geometrical features of the ribs used in the 1st and 2nd legs are: square section with rounded edges and base fillet, rib pitch/height of 8 and inclined at 60° with respect to the radial direction. Their blockage effect inside both 1st and 2nd leg is about 10%.

The test model differs with respect to the real design only because there is no curvature due to the blade camber. Conversely, the correct stagger angle of the real blade (60° with respect to the peripheral velocity) is preserved.

The model is machined out of Plexiglas, successively polished to ensure a good transparency. The minimum wall thickness is about 20mm, which is sufficiently high to allow for the correct application of the Transient Liquid Crystal Thermography (TLCT) technique.

TEST FACILITY AND MEASUREMENT TECHNIQUE

The experiments were performed on the rotating channel facility inside the Turbomachinery and Energy Conversion System Laboratory of the University of Udine. The rig has been designed with the specific purpose to obtain spatially resolved heat transfer coefficient distributions inside cooling channel models of complex geometries and by means of TLCT

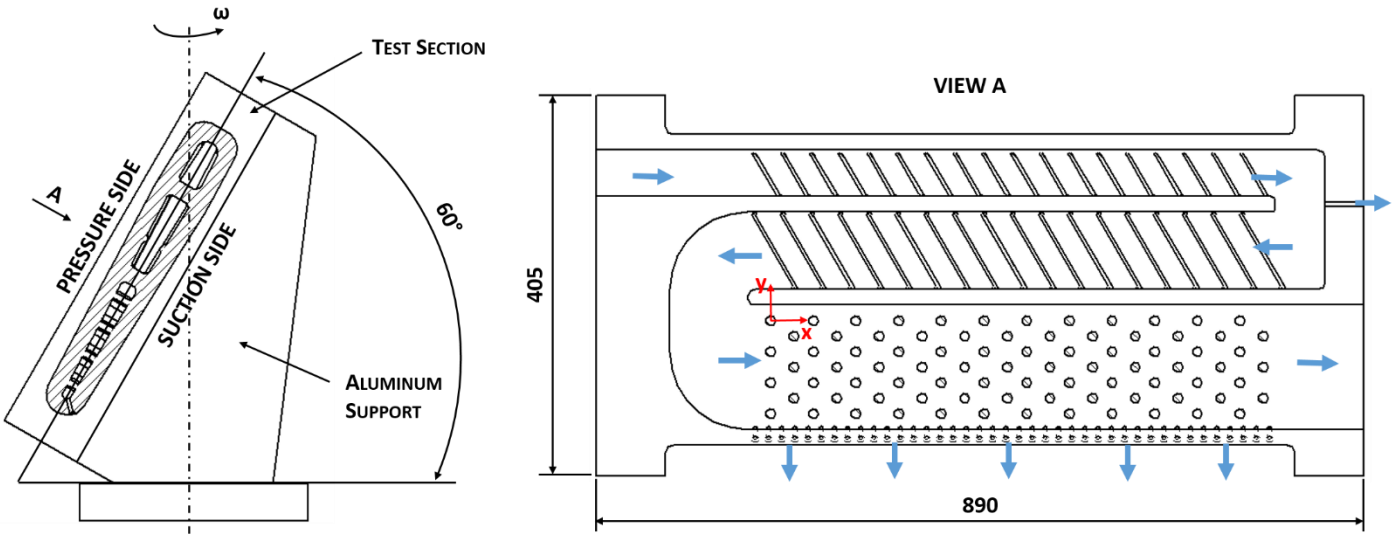

Figure 1: Test section sketch (dimensions in mm)

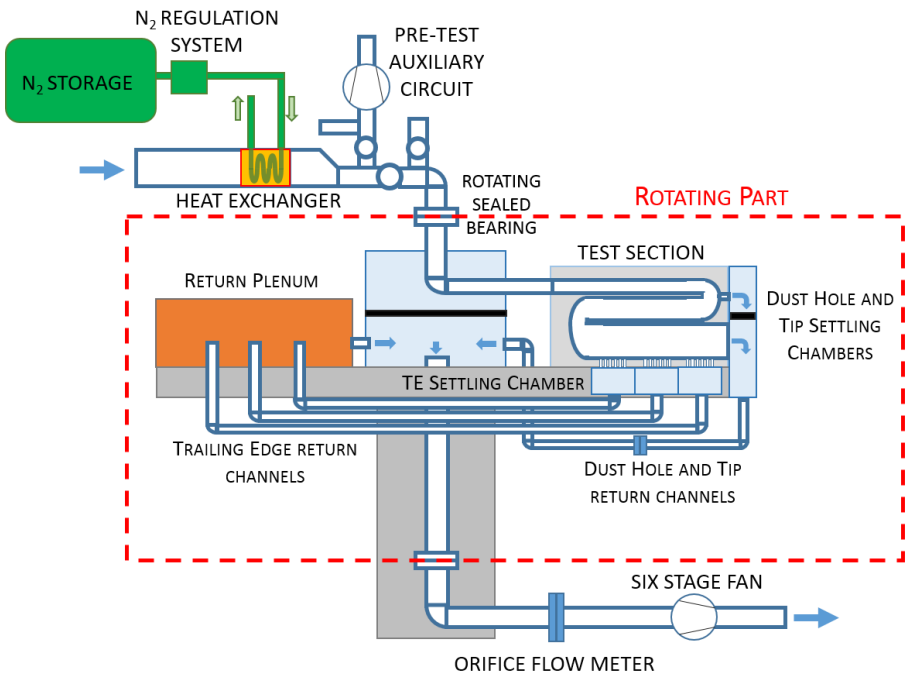

Figure 2: Air circuit sketch

technique. All the details are available in the Part 1 of this contribution [23].

In the following, only the information about the installation on the rig and working conditions of this specific geometry are reported.

The test section is installed on one side of the rotating arm at the blade stagger angle by means of two aluminum supports (see Fig. 1), while on the opposite side counterweights are used in order to balance the whole structure during rotation.

Flow is drawn through the rotating test section by a six stage centrifugal fan that sucks air from the test section through the rotating joint (see Fig. 2). The air flow rate is continuously monitored by an orifice flow meter installed in between the rotating joint and the fan.

As reported above, the test section is characterized by multiple discharges. A correct flow split between them must be ensured during stationary and rotating test, in order to reproduce real working conditions. For the tip discharges (1st leg dust hole and 3rd leg tip hole), the coolant exits the test section in a dedicated settling chamber, from where the flow is collected by means of instrumented pipes towards a main settling chamber placed at the center of the rotor and connected to the rotating electro-fluidic joint (see Fig. 2). On the two collecting pipes, calibrated orifice flow meters are installed to measure the airflow rate from dust hole and 3rd leg tip discharge hole, respectively. The correct flow split can be set by acting on gate valves.

A different solution has been used to control the distributed coolant flow extraction along the trailing edge holes. Each hole is connected to a settling chamber (trailing edge (TE) settling chambers in Fig. 2), which is divided in three regions accordingly to the main blade zones, namely hub, mid, and tip. The settling chambers discharge the air in a return plenum (see Fig. 2) placed on the opposite side of the rotating arm. The three connection pipes extract and deliver the coolant at the same radial position. By doing so, when the test section is spun, the same pressure gradient due to rotation is seen by each return line. Consequently, the same flow split of the static case will be automatically achieved.

Heat transfer measurements on the test section are carried out by means of thermochromic liquid crystals with the well-known transient technique. The fundamentals of the technique can be found in [24-26], while the specific methodology used in this work is reported in [23]. A mix (50% in volume) of two narrow banded encapsulated liquid crystals supplied by Hallcrest has been used, namely R2C1W and R12C1W (in the following named LC2 and LC1, respectively). The selection of these activation temperatures (2°C and 12°C) is the result of a trade-off between different requirements:

- liquid crystal activation must occur inside all the passage legs;
- keep the activation time below the maximum allowable test duration to ensure the validity of the 1D thermal diffusion hypothesis inside the model wall, which is at the basis the transient technique [24-26].

Moreover, another requirement for LC1 and LC2 identification was the value of the experimental parameter Θ, the "non dimensional temperature". According to [27], the non dimensional temperature parameter is defined as:

$$\Theta = \frac{T_w - T_i}{T_b - T_i} \quad (1)$$

and its value should be kept in the range 0.3-0.7 in order to minimize the data uncertainty.

Liquid crystal calibration has been performed ex-situ on a calibration plate [23] where the effects of the mixing of the two liquid crystals has been also checked and shown not to affect the liquid crystals optical properties. More complex in-situ calibration is not required since narrow banded liquid crystals are used (1°C of activation range) and, therefore, accuracy issues related to viewing and illumination angles are negligible. However, additional care was also taken in order to replicate the same viewing and lightning setup in both calibration and test facilities.

Regarding the choice of the lighting setup, its definition results from the need to illuminate properly and uniformly the test surface, to avoid light reflection, and to minimize radiation effects from the halogen lamps. Preliminary tests were conducted to evaluate the radiative effects of the halogen lamps on the test section. The lamps, set at different distances and angles, radiated a sample of the same plastic material and thickness of which the test section is made. The internal surface was placed over an insulating material, hence providing an adiabatic boundary condition that highlights the radiative effects. The latter was quantified by measuring the surface temperature by two thermocouples over a time of 120s. Results of these tests allow to determine the lamps positions and orientation (with respect to the test section external surface) in order to limit the radiative effect below 20% of the one obtained with perpendicular lamps at 20 cm from the surface.

The vision system that is used to acquire the images of the liquid crystals is installed on board of the rotating arm. Two Basler acA1300-60gc cameras are used to frame the full channel surface. The cameras are connected to a fan-less PC, installed on board, that has the function to control the acquisition and store the images. The wide angle of view of the camera optics produces distorted images that must be de-warped in order to fit the image space onto the CAD space. A dedicated procedure has been developed for the purpose and is described in details in [23].

Flow temperature values inside the model are acquired by means of K-type thermocouples (TC). This type of sensor has been selected because of their good sensitivity in the measurement range (-90°C/+30°C). The 'hot' junction diameter is about 0.075mm, which is a good compromise between response time, cost and market availability. A set of 30 thermocouples were installed in the test section in the positions shown in Fig. 3. Multiple TCs have been installed at the start and at the end of each leg in order to have a full characterization of the temperature evolution at the legs boundaries. In order to increase the accuracy of the temperature field reconstruction, additional TCs have also been installed at about mid length of each leg.

TEST CONDITIONS AND DATA REDUCTION

Detailed heat transfer maps have been obtained on both pressure and suction sides of the channel. Tests have been carried out at Re = 21000 and Ro = 0 and 0.074, both defined at inlet of the 1st leg:

Figure 3: Thermocouple location

$$\mathrm{Re} = \frac{\rho U_b \mathrm{d_h}}{\mu} \quad (2)$$

$$\mathrm{Ro} = \frac{\Omega \mathrm{d_h}}{U_b} \quad (3)$$

$$d_h = \frac{4 \text{ cross section area}}{\text{cross section perimeter}} \quad (4)$$

Both Reynolds and rotation numbers values are consistent with those that can be found inside land based gas turbines. Concerning the buoyancy parameter:

$$\mathrm{Bo} = \frac{\Delta\rho}{\rho}\mathrm{Ro}^2\frac{\mathrm{R}}{\mathrm{d_h}} = \frac{\mathrm{T_w}\text{-}\mathrm{T_b}}{\mathrm{T_b}}\mathrm{Ro}^2\frac{\mathrm{R}}{\mathrm{d_h}} \quad (5)$$

it has to be considered that the present experiments are made with a transient approach, i.e. with a continuous change in fluid and wall temperature, both during time and along the passages. Therefore, the definition of a reference Bo of the tests is not straight forward, which is the main drawback of the transient technique. However, for the present experiments, considering the geometrical and working characteristics, the Bo values are low. To give an example, the Bo at the inlet of the test section, at the beginning of the temperature step is about 0.02. Therefore, buoyancy effects are expected to be negligible in the present configuration.

Tests in static condition have been performed to assess the reliability of the developed measurement procedure. This is done by comparing the results obtained by the two crystals and with different evolutions of the flow temperature, which have been obtained by different settings of the cooling system (T_{he} = 5°C, and -15°C). In this way, the time response of the liquid crystal mixture is varied significantly, hence the robustness and accuracy of the measurement and processing procedure could be tested. A summary of all tested conditions is provided in Table 1.

Table 1: Test conditions

Re = 21000		**Ro =0**	**Ro = 0.074**
T_{he} = -15°C	PS	x	x
	SS	x	x
T_{he} = +5°C	SS	x	

The following definition of the Nusselt number has been used to non-dimensionalize the computed heat transfer coefficient distributions:

$$Nu = \frac{HTC\ d_h}{k} \quad (6)$$

The specific hydraulic diameter of each legs was used as reference length for the calculations. The thermal conductivity of the fluid was modelled at every positions considering the time-averaged fluid temperature evolution until the liquid crystal indication took place [25].
Data normalization is performed using as reference Nusselt number the smooth channel value from classical Dittus-Boelter correlation:

$$Nu_0 = 0.023 Re^{4/5} Pr^n \quad (7)$$

where n = 0.4 for cooling processes. The Nu_0 value is computed at the inlet of the test section and kept constant throughout the channel.

RESULTS

PRELIMINARY TESTS AND DATA VALIDATION

In literature, it is possible to find different contributions about the analysis of the uncertainties in thermochromic liquid crystal measurements with the application of a transient approach.
The majority of those are based on a strong assumption that is the adoption of an ideal step-change in fluid temperature. In particular, in [27] it is suggested that the non-dimensional temperature Θ should fall in a certain interval of values in order to guarantee the minimum uncertainty in the computation of HTC. Hence, if the fluid initial and step temperatures are known, the best suited liquid crystals activation temperature can be calculated and an estimation of the uncertainty on the HTC values can be provided. However, this fully analytic approach is based on the unrealistic assumption of an ideal step where Θ is uniquely determined. Conversely, in transient experiments the fluid temperature and the respective non-dimensional temperature are not constant during the test. To overcome this limitation, in [28] the uncertainty analysis is based on a hypothetical ideal fluid temperature step that provides the same liquid crystal activation time as from the real fluid temperature history.
In this contribution, instead of pursuing the numerical approach for the uncertainty analysis with the limitations of above, it has been decided to exploit the rotating rig capabilities and assess the validity of the presented results through an empirical approach, which is considered to be more reliable.
More precisely, tests have been conducted with very different boundary conditions (such as cold step temperature) and the resulting HTC have been compared. This type of analysis not only confirms the repeatability of the experimental technique, but also allows a quantitative estimation of the integrated effects of all error sources. Indeed, the analysis of the results obtained with a single liquid crystal for different temperature steps or the

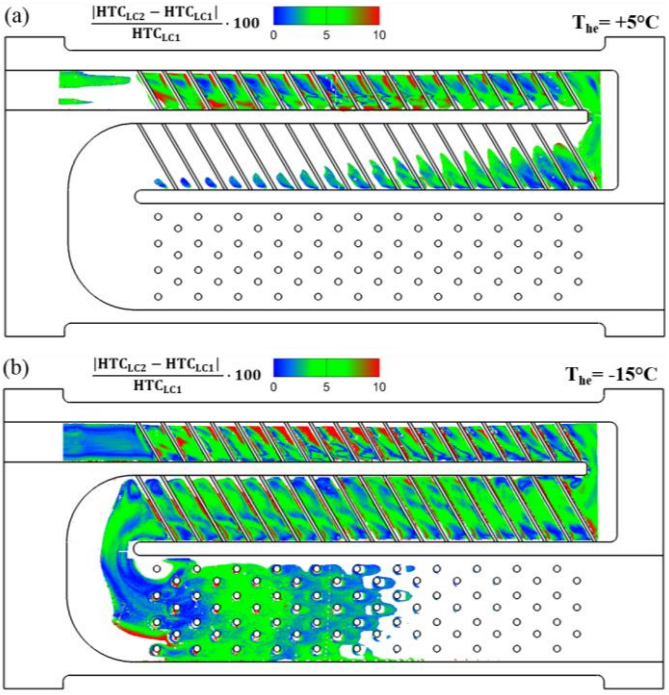

Figure 4: Differences in the measured HTC values from the two liquid crystals LC1 and LC2 and with different flow temperature evolutions (a) T_{he}=5°C, (b) T_{he}=-15°C

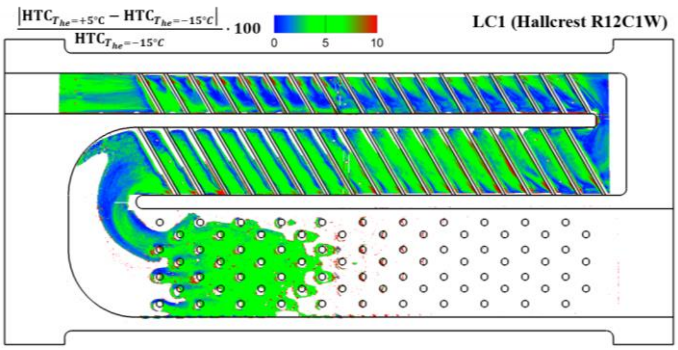

Figure 5: Differences in the measured HTC values from liquid crystals LC1 with different flow temperature evolutions

analysis of the results obtained from two different liquid crystals at the same temperature step allows to highlight the measurement errors that can be generated by:

- uncertainty on the measurement of T_b;
- uncertainty on the measurement of T_w;
- uncertainty on the time detection;
- uncertainty on the determination of the material physical properties.

Figure 4 reports the difference of HTC distribution obtained by LC1 and LC2 for the test performed with the different temperature steps. The data have been acquired on the SS only

and in static condition. For the hotter step (T_{he}=5°C, Fig. 4-a), the comparison is limited to the 1st leg and a portion of the 2nd one because LC2 does not activate within the test time. For both test conditions the comparison reveals that the results from the two LC are consistent, being the difference generally limited to 5%, which is far below the standard accuracy of the method. Only for the colder step (T_{he}=-15°C, Fig. 4-b), wider zone with differences above 10% can be found inside the 1st leg. This is associated to the very fast activation of LC1 that occurs with this temperature step and that reduces substantially the accuracy of the indication from this liquid crystal.

The effect of the step evolution is provided in Fig. 5 for LC1. Again, the differences are limited to 5%, with only small areas of higher values localized in the region of flow impingement downstream of each rib inside the 1st and 2nd legs, however limited to less than 10%.

Considering the results just presented, it was decided to run the experiments with always the same temperature step (the one set by the initial condition of T_{he}=-15°C). The indications by LC2 are used to compute the HTC values inside the 1st leg, while LC1 is used for the successive 2nd and 3rd legs. With these choices, the uncertainty can be assumed below 10% over the whole channel.

STATIC CHANNEL, RO = 0

Figure 6 reports the Nu distribution maps on both PS and SS obtained for the static channel condition.

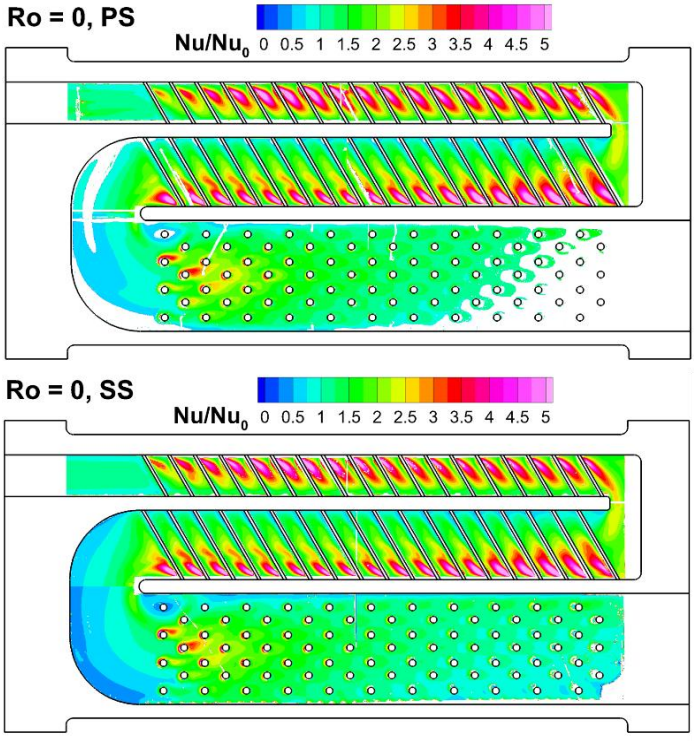

Figure 6: Nu/Nu_0 maps on pressure (top) and suction (bottom) sides of the channel for the static case

At first, an overall agreement between data on PS and SS can be appreciated, as expected in view of the perfect symmetry of the passage. However, a better comparison is made by means of the Nu profiles extracted along the legs centerlines and reported in Fig. 7. The profiles comparison shows a very good matching between PS and SS Nu/Nu_0, which confirms the good reliability of the presented data.

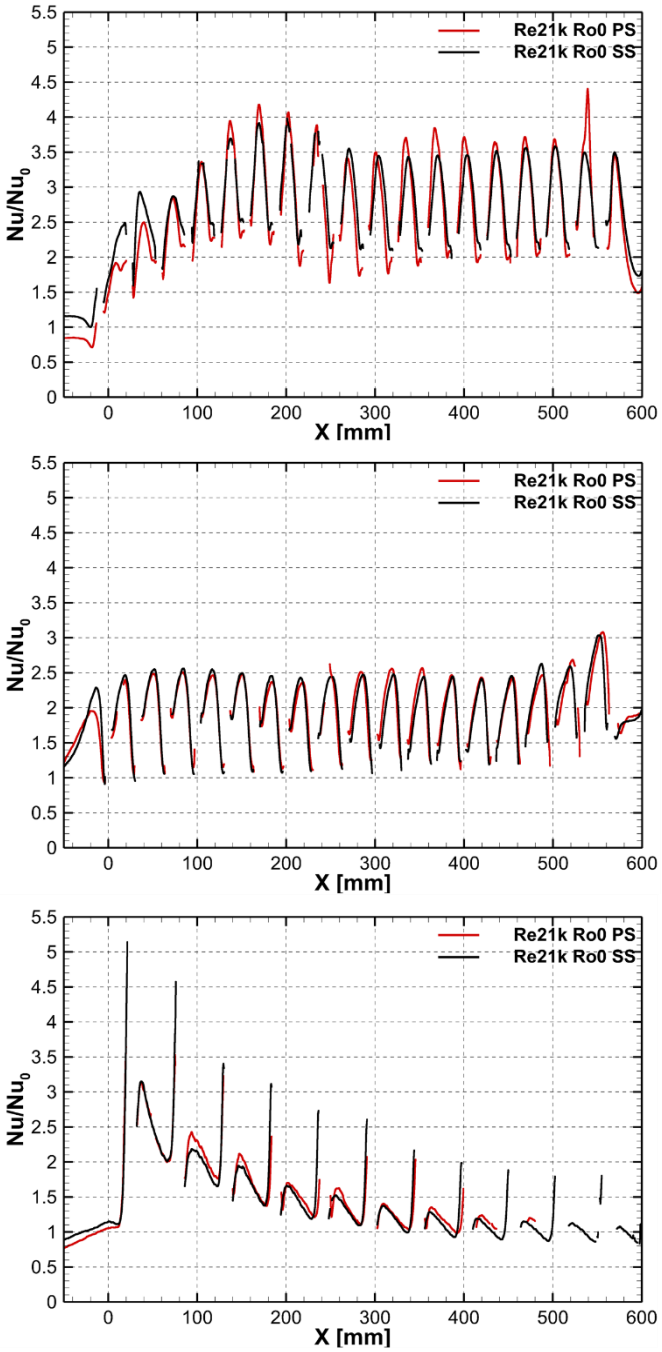

Figure 7: Comparison of Nu/Nu_0 profiles on PS ans SS extracted along the legs centerlines: first leg (top), second leg (center) and third leg (bottom)

Concerning the 1st leg, regions of high heat transfer are found downstream of each ribs, the guiding effects of the inclined ribs is also well in evidence by the contours of the Nu/Nu_0 (Fig. 6). As expected, an overall enhancement with respect to the smooth channel case is observed on the whole channel surface thanks to the turbulent mixing produced by the ribs [6, 11]. The same enhancement (about 1.5) is also found in the first 180° turn, at least in the measured area (the outer portion of the curve was not optically accessible). Inside the 2nd leg, the behavior is similar but with the difference that the thermal field development is affected by the flow evolution after the bend. Indeed, it is well known that 180° turns without vanes (as in the present case) determine an acceleration of the fluid layer on the external side of the path with flow separation close to inner corner [18, 19]. Downstream the turn, the flow will progressively recover from separation and it will develop towards a more uniform flow distribution over the channel span. This behavior is confirmed by the present data. Regions of low Nu are found close to the lateral wall that separates from the first leg, the minimum being located close to the U-bend corner. A detail of the effect of this flow separation on the heat transfer behavior can be appreciated in Fig. 8. The highest Nu, extending on the wider areas, are found downstream of the first ribs of the leg. Afterwards the flow tends to recover a more uniform velocity distribution and therefore its separation above the obstacles is less intense with a consequent reduction of Nu.

Inside the 3rd leg, again flow separation is found close to the corner of the bend, as can be appreciated by the very low Nu values that are found around the first pin fin (Figs. 6, 8). The Nu values are higher at the beginning of the leg and they lower moving towards the blade tip due to the progressive flow discharge at the trailing edge that reduces the local Reynolds number, in agreement with previous observations [14]. The literature about pin fin roughened channels with lateral discharge [14-16] reports a local augmentation of heat transfer coefficient in proximity of each exhaust hole/slot, due to the local flow acceleration. This effect cannot be seen in the present channel configuration. The number of discharge holes is very high (40) and the local amount of exhausted flow rate is consequently low. Local flow acceleration in the hole proximity is therefore not that strong to leave a footprint on the heat transfer field.

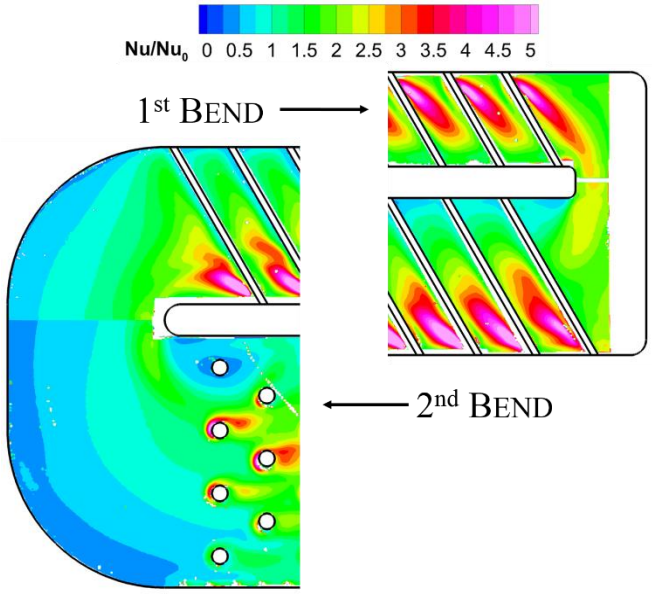

Figure 8: Details of the Nu distribution around the bend regions on SS at Ro=0

ROTATING CHANNEL, RO = 0.074

The Nusselt distribution maps obtained for the rotating channel case are reported in Fig. 9. Obviously, the same main features that were commented about the static case characterize the rotating heat transfer fields. However, the expectation is to find differences in some local features that can be directly related to rotational effects. In the introduction, a review about the rotational effects on radial channels has been made. Briefly, in a radial channel with outward flow, the secondary structures set by rotation produce a reduction of the heat transfer on the channel leading wall (SS) and, conversely, an augmentation on the trailing wall (PS). If the flow is radially inward, the behavior is the opposite. With this mind, in the present case by comparing static and rotating data one should expect:

- higher Nu in rotation on PS of 1st and 3rd leg, and on SS of 2nd leg;
- lower Nu in rotation on SS of 1st and 3rd leg, and on PS of 2nd leg.

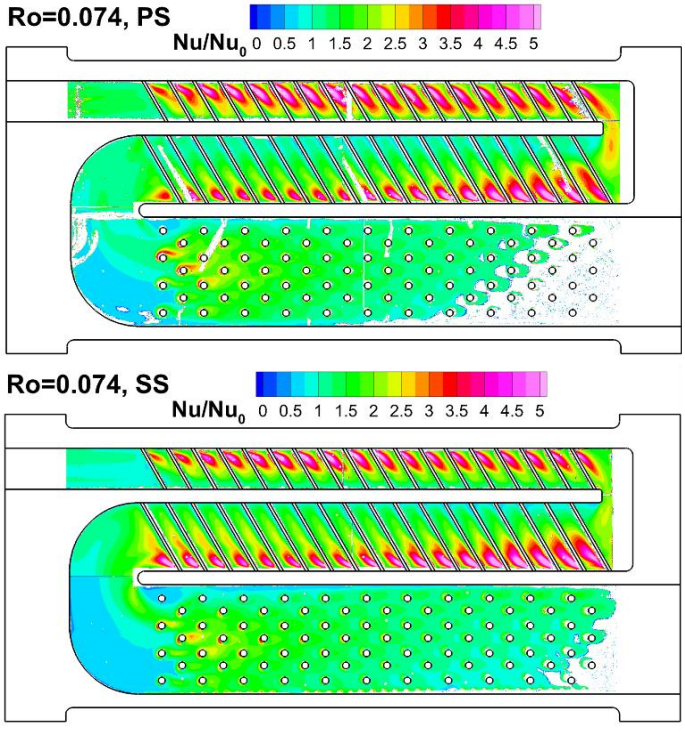

Figure 9: Nu/Nu_0 maps on pressure (top) and suction (bottom) sides of the channel for the rotating case

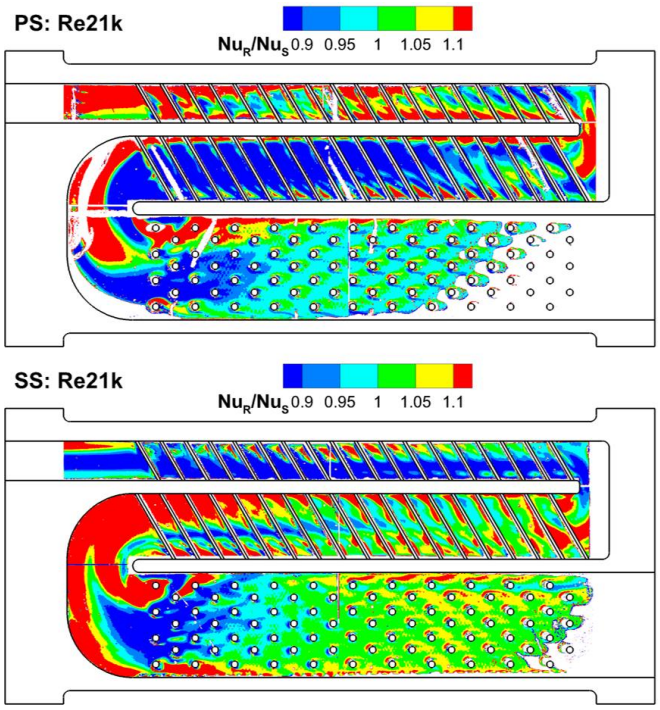

Figure 10: Nu_R/Nu_S distribution on pressure (top) and suction (bottom) sides

These effects are only partially confirmed by an initial comparison of Fig. 9 with Fig. 6. A better comparison is made with the data in Fig. 10 that shows the ratio between the Nu values measured in rotating and static conditions. Indeed, an overall reduction of heat transfer can be appreciated inside the 1st leg on SS and inside the 2nd leg on the PS. Conversely, smaller variation between static and rotating conditions can be found inside 1st leg PS and 2nd leg SS, where a positive effect of rotation should be found. This behavior, unexpected with respect to the consolidated knowledge, can be explained by looking at the physics that is behind the generation of the rotation induced secondary structures.

As already reported in the introduction, the Coriolis structure formation and development is mainly a mechanism that is driven by the equilibrium between the forces associated to Coriolis acceleration and the induced pressure gradient. Inside the near wall flow layers, this equilibrium is unbalanced towards the pressure forces, which therefore displace the near wall flow towards the leading side of the channel. In the present case, the situation that is set is depicted in Fig. 11. The sketch refers to the 1st leg flow configuration, where it can be seen how the misalignment between channel cross section axis and rotation axis leads to the onset of Coriolis structures that does not separate or reattach on the channel lateral walls. Indeed, in view of the physical mechanism behind the phenomenon, separation and reattachment can only exist at the external limits of the cross section. In the present case, the scenario is further complicated by the fact that the separation has to take place on a concave surface (the rounded wall on the upper part of the channel section, made to accommodate inside the blade leading edge).

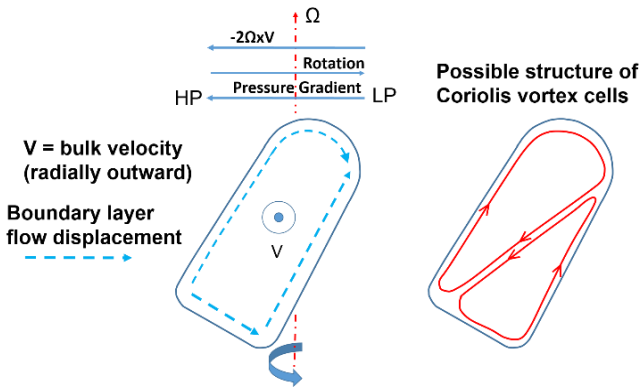

Figure 11: Flow behavior induced by Coriolis acceleration and pressure gradient

Separation position, which is therefore not easy to be determined, is likely to be characterized by an unsteady nature. In addition, the Coriolis vortex cells have to interact with the secondary structures induced by the ribs, making the conjecture of the overall secondary flow structure quite challenging. Again, the data provided by CFD and flow measurements planned for the near future will help to better understand this behavior. Hence, it appears that no flow reattachment of secondary structures will take place on the trailing wall (PS), which justifies the evidence that the heat transfer on that side is not positively influenced by rotation.

The same phenomenology applies to the SS of the 2nd leg.

Inside the 3rd leg, the behavior is more complex with regions of local augmentation or reduction of the Nu values both inside the PS and SS. A local reduction of Nu is observed in the first portion of the leg on both PS and SS. Conversely, rotation has a positive effect on the flow re-circulating region immediately downstream of the turn and close to the dividing wall, where very low values of Nu were found for the static case (see Fig. 8). After the first 4-5 rows of pins, the Nu starts to recover and remains comparable to the static case on the PS while the SS shows a modest increase near the tip. This behavior must therefore be associated to the complex forces induced by rotation acting on the separated flow that surround the pin-fins, which is already intrinsically three dimensional in view of the short aspect ratio of the turbulators. A detailed analysis of the flow field inside the rotating pin-fin matrix is required in order to understand this phenomenon, however this data are not available at present.

AREA-AVERAGED DATA

Final comments are provided by looking at area-averaged data, which help to have an overall estimate of the effects that rotation produces inside this channel configuration.

Figure 12 shows the area average distribution through the first two passages. Nusselt data have been averaged for each inter-rib area, as depicted in Fig. 12. With respect to the contribution of Wagner et al. [29], it can be appreciated a good consistency in the trends of the Nu/Nu_0 distribution along the first passage. In the second passage, instead, a different trend is observed. In the present case, a substantial reduction of the Nu/Nu_0 values is

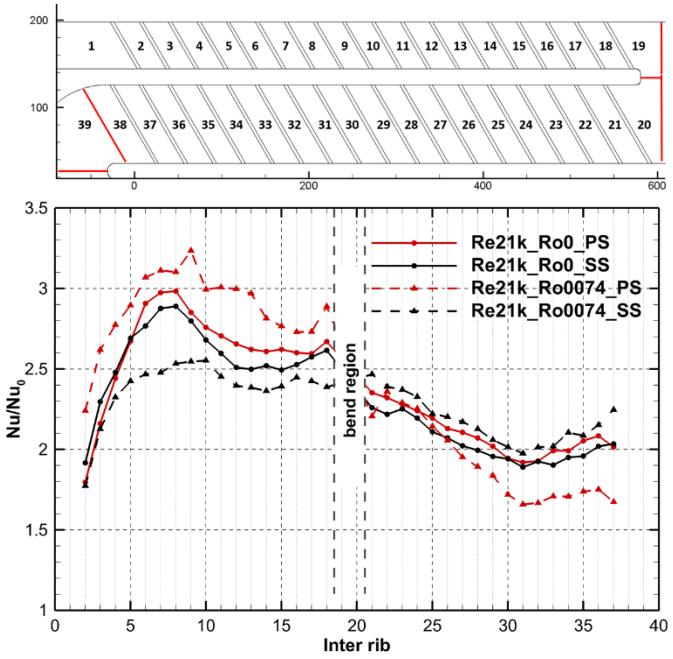

Figure 12: Detailed distribution of Nu/Nu_0 area averages for each inter rib region.

found after the bend while in the data of Wagner et al [29] immediately after the bend values of Nu/Nu_0 up to 3.5-4 are reported. An explanation for this different behavior can be ascribed to the different geometry of the bend region. In the present experiments, the enlargement of the channel cross section, thus the change of the hydraulic diameter, and the mass flow extraction from the dust hole, causes a local Reynolds number decrease that can be the cause of the observed reduction of enhancement after the 180° turn.

Overall performances of the passages at varying the working conditions can be deduced by looking at the area average of Nu numbers inside each legs, computed on the whole surfaces but excluding the 180° turns. In other words, by doing the average of the data obtained from Fig. 12 from section 2 to 18 for the first passage and from section 21 to 37 for the second passage. Data average on the third passage has been evaluated considering the region after the 180° turn and excluding the pins. The resulting values are given in Table 2.

It can be appreciated again the good consistency of the data acquired on PS and SS for Ro=0. Rotation determines an overall reduction of the heat transfer capabilities of about 7-9% on the 1st leg SS and 2nd leg PS. On the contrary, an augmentation of 5-8% is found on the opposite surfaces.

Concerning the 3rd leg, from an area averaged point of view, its thermal behavior is not affected by rotation, differently from the results reported by [14] where rotational effects where clearly evident also on the area averaged data. This different behavior may be due to the different inlet conditions to the pin fin channels (smooth and radial for [14], 3rd passage fed by a 180°bend in the present case) and the higher Ro that characterizes the analysis performed in [14].

Table 2: Area averaged data

Nu/Nu_0	Ro = 0		Ro = 0.074		Nu_R/Nu_S	
	PS	SS	PS	SS	PS	SS
1 LEG	2.69	2.57	2.90	2.38	1.08	0.93
2 LEG	2.11	2.05	1.92	2.16	0.91	1.05
3 LEG	1.40	1.37	1.39	1.35	0.99	0.99

CONCLUSIONS

The contribution reports the first results obtained on a new rig that has been specifically designed to perform heat transfer measurements inside complex models of cooling channels for gas turbine blades.

The investigated geometry is a three-pass channel, rib roughened in the first two legs and provided with short pin fins and distributed coolant discharge in the 3rd leg. Geometrical features such as channel cross section, rounded edges, contoured rib, and filleted pin fins have been used in order to resemble as close as possible a realistic geometry. Tests have been performed at working conditions resembling those of land-based gas turbines, namely Re=21000 and Ro=0, and 0.074. A realistic channel orientation was also considered by spinning the test section at 60° with respect to the peripheral velocity.

Spatially resolved heat transfer maps highlighted the effects of rotation. A consistent detrimental effect on the Nu values has been found inside the 1st leg SS and 2nd leg PS, while on the opposite walls (1st leg PS and 2nd leg SS), an increment of the heat transfer is found with respect to the static case. This behavior is explained by the combined effect of the present channel orientation and cross-section. Inside the pin fins roughened 3rd leg, rotation has complex and localized effects, but the area averaged Nu values remains practically unchanged between static and rotating conditions, confirming previous contributions.

Future testing at different working conditions are planned in order to exploit the capabilities of the newly available rig in characterizing the effects of rotation on turbine blade cooling designs.

PERMISSION FOR USE

REFERENCES

[1] Hart, J.E., 1970, “Instability and secondary motion in a rotating channel flow”, J. Fluid. Mech., 45, pp. 341–351

[2] Lezius, D.K. and Johnston, J.P., 1976, “Numerical study of viscous flow in rotating rectangular ducts”, J. Fluid. Mech., 77, pp. 153–176

[3] Speziale, C.G., 1982, "Numerical study of viscous flow in rotating rectangular ducts", J. Fluid. Mech., 122, pp. 251–271
[4] Speziale, C.G. and Thangam S., 1983, "Numerical study of secondary flows and roll-cell instabilities in rotating channel flow", J. Fluid. Mech., 130, pp. 377–395.
[5] Wagner, J.H., Johnson, B.V., Graziana, R.A. and Yeh, F.C., 1992, "Heat Transfer in Rotating Serpentine Passages with Trips Normal to the Flow", ASME J. Turbomachinery, Vol. 114, pp. 847-857.
[6] Zhou, F. and Acharya, S., 2008, "Heat Transfer at High Rotation Numbers in a Two-Pass 4:1 Aspect Ratio Rectangular Channel with 45 deg Skewed Ribs", ASME J. Turbomachinary, Vol. 130, pp. 021019-1-021019-2
[7] Pascotto, M., Armellini, A., Mucignat, C. and Casarsa, L., "Coriolis effects on the flow field inside a rotating triangular channel for leading edge cooling", 2014, ASME J. Turbomach., 136(3), p031019
[8] Furlani, L., Armellini, A. and Casarsa, L., "Buoyancy effects at high rotation number on the flow field inside a triangular shaped rib roughened channel", 2015, ETC11
[9] Coletti, F., Lo Jacono, D., Cresci, I. and Arts, T., "Turbulent flow in rib-roughened channel under the effect of Coriolis and rotational buoyancy forces", 2014, Physics of Fluids 26, p. 045111
[10] Dutta, S. and Han, J.C., 1996, "Local Heat Transfer in Rotating Smooth and Ribbed Two-Pass Square Channels with Three Channel Orientations", ASME J. Heat Transfer, Vol. 118, pp. 578-584.
[11] Huh, M., Lei, J. and Han, J.C., 2010, "Influence of Channel Orientation on Heat Transfer in a Two-Pass Smooth and Ribbed Rectangular Channel (AR=2:1) under Large Rotation Numbers", ASME Paper No. GT2010-22190.
[12] Chyu, M., Hsing, Y. and Natarajan, V., 1998, "Convective heat transfer of cubic fin arrays in a narrow channel". Journal of Turbomachinery, 120, pp. 362–367.
[13] Metzger, D., Fan, C. and Haley, S., 1984, "Effects of pin shape and array orientation on heat transfer and pressure loss in pin fin arrays", Journal of engineering for power, 106(1), pp. 252–257.
[14] Rallabandi, A.P., Liu, Y.H. and Han, J.C., 2010, "Heat transfer in trailing edge wedge-shaped pin fin channel with slot ejection under high rotation numbers", Proc. ASME Turbo-Expo 2010, GT2010-22832.
[15] Willett, F. and Bergles, A., 2002, "Heat transfer in rotating narrow rectangular pin-fin ducts", Experimental Thermal and Fluid Science, 25(7), pp. 573–582.
[16] Chang, S., Yang, T., Hong, G.F. and Liou, T., 2008, "Heat Transfer in Radially Rotating Pin-Fin Channel at High Rotation Numbers", Proc. ASME Turbo-Expo 2008, GT2008-50514.
[17] Qiu, L., Deng, H. and Tao, Z., 2012, "Effect of channel orientation in a rotating wedge-shaped cooling channel with pin fins and ribs", Proc. ASME Turbo-Expo 2012, GT2012-68439
[18] Lei, J., Su, P., Xie, G. and Lorenzini, G., 2016, "The effect of a hub turning vane on turbulent flow and heat transfer in a four-pass channel at high rotation numbers", 2016, International Journal of Heat and Mass Transfer, vol. 92 pp 578-588
[19] Lei, J., Li, S.J., Han, J.C., Zhang, L. and Moon, H.K., 2013, "Heat transfer in rotating multi-pass rectangular smooth channel with and without a turning vane in hub region", Proc. ASME Turbo-Expo 2013, GT2013-94269
[20] Bailey, J.C. and Bunker, R.S., 2003, "Heat Transfer And Friction in Channels With Very High Blockage 45° Staggered Turbulators", Proc. ASME Turbo-Expo 2003, GT2003-38611
[21] Taslim, M.E. and Spring, S.D., 1994, "Effects of Turbulator Profile and Spacing on Heat Transfer and Friction in a Channel", AIAA J. Thermophysics and Heat Transfer, Vol. 8(3), pp 555-562
[22] Chandra, P.R., Fontenot, M.C. and Han, J.C., 1998, "Effect of Rib Profiles on Turbulent Channel Heat Transfer", AIAA J. Thermophysics and Heat Transfer, Vol. 12, pp116-11
[23] Pagnacco, F., Furlani, L., Armellini, A., Casarsa, L. and Davis, A., 2015, "Rotating heat transfer measurements on a multi-pass internal cooling channel – I Rig Development", Submitted to ASME Turbo Expo 2016 GT2016-56308
[24] Ekkad, S. and Han, J.C., 2000, "A transient liquid crystal thermography technique for gas turbine heat transfer measurements", Meas. Sci. Technol. 11 957-968
[25] Poser, R., von Wolfersdorf, J. and Lutum, E., 2007, "Advanced evaluation of transient heat transfer experiments using thermochromic liquid crystals", Journal of Power and Energy, Vol 221 DOI: 10.1243/09576509JPE464
[26] Ireland, P.T. and Jones, T.V., 2000, "Liquid crystal measurements of heat transfer and surface shear stress", Meas. Sci. Technol. 11 969-986
[27] Yan, Y.Y. and Owen, M., 2002, "Uncertainties in transient heat transfer measurements with liquid crystal", International Journal of Heat and Fluid Flow 23(2002) 29-35
[28] Waidmann, C., Poser, R. and von Wolfersdorf, J., 2013, "Application of thermochromic liquid crystal mixtures for transient heat transfer measurements", 10th European Conference on Turbomachinery, ISBN978-952-265-385-7 p.685-696
[29] Wagner, J.H., Johnson, B.V., Graziana, R.A. and Yeh, F.C., 1994, "Heat Transfer in Rotating Serpentine Passages with Trips Skewed to the Flow", ASME J. Turbomachinery, Vol. 116, pp. 113-123.